Human Molecular Genetics, 2003, Vol. 12, No. 5 **497–508**
DOI: 10.1093/hmg/ddg046

Specific progressive cAMP reduction implicates energy deficit in presymptomatic Huntington's disease knock-in mice

Silvia Gines, Ihn Sik Seong, Elisa Fossale, Elena Ivanova, Flavia Trettel[†], James F. Gusella, Vanessa C. Wheeler, Francesca Persichetti and Marcy E. MacDonald*

Molecular Neurogenetics Unit, Massachusetts General Hospital, Building 149, 13th St, Charlestown, MA 02129, USA

Received October 23, 2002; Revised and Accepted December 20, 2002

Defects in gene transcription and mitochondrial function have been implicated in the dominant disease process that leads to the loss of striatal neurons in Huntington's disease (HD). Here we have used precise genetic HD mouse and striatal cell models to investigate the hypothesis that decreased cAMP responsive element (CRE)-mediated gene transcription may reflect impaired energy metabolism. We found that reduced CRE-signaling in *Hdh^{Q111}* striatum, monitored by brain derived neurotrophic factor and phospho-CRE binding protein (CREB), predated inclusion formation. Furthermore, cAMP levels in *Hdh^{Q111}* striatum declined from an early age (10 weeks), and cAMP was significantly decreased in HD postmortem brain and lymphoblastoid cells, attesting to a chronic deficit in man. Reduced CRE-signaling in cultured ST*Hdh^{Q111}* striatal cells was associated with cytosolic CREB binding protein that mirrored diminished cAMP synthesis. Moreover, mutant cells exhibited mitochondrial respiratory chain impairment, evidenced by decreased ATP and ATP/ADP ratio, impaired MTT conversion and heightened sensitivity to 3-nitropropionic acid. Thus, our findings strongly suggest that impaired ATP synthesis and diminished cAMP levels amplify the early HD disease cascade by decreasing CRE-regulated gene transcription and altering energy dependent processes essential to neuronal cell survival.

INTRODUCTION

In Huntington's disease (HD), an elongated glutamine tract at the amino terminus of huntingtin leads to the loss of vulnerable neurons, primarily in the striatum, and to chorea, cognitive and psychiatric decline (1). Huntingtin is a large nuclear and cytoplasmic HEAT domain protein that has been implicated in mRNA production (2–5) and vesicle trafficking (2,6–10). The polyglutamine expansion appears to confer a novel structural property on mutant huntingtin that does not impair the protein's essential developmental activities (11), but which instead triggers a dominant disease process (12).

HD-like neuropathology in animals treated with mitochondrial toxins and loss of mitochondrial respiratory chain activities in end-stage HD patient brain (13) have suggested that energy deficits might contribute to the disease process (reviewed in 14). However, studies with HD transgenic systems have implicated decreased transcription of genes regulated by cyclic adenosine 3′,5′-monophosphate (cAMP) responsive element (CRE) binding protein (CREB) (15–19). These genes include brain derived neurotrophic factor (BDNF) (20) and a host of others involved in diverse processes ranging from neurotransmission (15,21) to cholesterol metabolism (22).

Reduced gene transcription has been ascribed to sequestration of coactivators that bind huntingtin amino terminus, such as CREB binding protein (CBP) or $TAF_{II}130$, into inclusions formed from mutant amino terminal product (16–19,23). However, CBP is localized to inclusions in distinct polyglutamine neurodegenerative disorders, DRPLA (18) and SBMA (24), implying that sequestration may be a downstream consequence of the disease process. Moreover, CBP sequestration seems unlikely to explain the dominant reduction in BDNF transcription observed in immortalized *STHdh^{Q111}* striatal cells (20), which accurately express normal and mutant huntingtin and do not exhibit amino terminal product inclusions (5).

An alternative possibility for diminished CRE-mediated gene transcription, which is linked to energy impairment, is a deficiency in cAMP, the second messenger in CRE-mediated

*To whom correspondence should be addressed. Tel: +1 6177265089; Fax: +1 6177265735; Email: macdonam@helix.mgh.harvard.edu
[†]Present address: Department of Pharmacology, University of Rome La Sapienza, P. le A Moro 5, I00185 Rome, Italy.

signaling. This scenario is supported by evidence for low cAMP in the cerebral spinal fluid of symptomatic HD patients (25), and by the capacity of forskolin, which stimulates adenylyl cyclases to produce cAMP from ATP, to ameliorate mutant huntingtin-fragment induced phenotypes in PC12 cells (19). Moreover, recent data suggests a direct impact of mutant huntingtin on mitochondrial function. Ectopic mutant huntingtin amino terminal fragment was able to induce deficits in calcium handling found in mitochondria isolated from HD patient lymphoblastoid cells (26,27) and HD transgenic mouse brain (27).

Consequently, we have used precise genetic HD mouse and striatal cell models to test the hypothesis that reduced cAMP may link aberrant CRE signaling and potential energy deficits early in the disease process. Hdh^{Q111} mice accurately express 111-glutamine mutant huntingtin and exhibit early dominant abnormalities selective for medium spiny striatal neurons, including nuclear retention of full-length mutant huntingtin (28). These changes predate late onset mutant amino terminal product (as inclusions and insoluble-aggregate), at ~12 months of age, and overt neurodegeneration, evident at ~24 months (28,29). The cognate immortalized STHdh^{Q111} striatal neuronal cell lines accurately express endogenous normal and mutant huntingtin and display dominant mutant phenotypes (5), including decreased BDNF transcription (20), consistent with aberrant PKA-CREB signaling *in vivo*.

Our results show for the first time that the dominant disease process triggered by mutant huntingtin features early, unremitting energy deficits, which are likely to amplify the disease cascade by affecting a host of homeostatic processes involved in cell survival.

RESULTS

Dominantly reduced PKA–CREB signaling and cAMP in Hdh^{Q111} brain

We first investigated whether, as suggested by decreased BDNF transcription in $STHdh^{Q111}$ striatal cells (20), altered cAMP PKA-CREB signaling might be an early consequence of the *HD* mutation *in vivo*. BDNF and phospho-CREB levels in extracts of dissected Hdh^{Q111} brain were assessed by immunoblot analyses at 5 months of age. The results, shown in Figure 1A, revealed that, when normalized to β-actin in the same lane, BDNF levels in cortical and striatal extracts from Hdh^{Q111} homozygotes were decreased from wild-type levels by 2.2- and 1.4-fold, respectively. Moreover, although total CREB levels were similar (data not shown), the level of the transcriptionally active form of CREB, phospho-CREB, in cortical extracts from Hdh^{Q111} homozygotes and heterozygotes was reduced, by 4.5- and 2.2-fold, respectively (Fig. 1B).

As these data supported dominantly diminished PKA/CREB signaling, we tested cAMP levels in cortical tissue extracts from Hdh^{Q111} homozygote and heterozygote mice. The results of the competitive enzyme immunoassay (EIA) (Fig. 1B histogram) revealed significantly reduced cAMP levels in Hdh^{Q111} homozygote (1.5-fold; $P < 0.001$) and Hdh^{Q111} heterozygote (1.2-fold; $P < 0.05$) extracts, compared with wild-type littermate extracts. These findings, therefore, demonstrated that the *HD* mutation led to a dominant reduction in cAMP by 5 months of age.

cAMP is selectively reduced early in the disease process

As the early Hdh^{Q111} disease process is progressive and selective for striatum, we next determined the timing and regional selectivity of decreased cAMP. EIA experiments were performed with striatum, cortex and cerebellum dissected from Hdh^{Q111} homozygote and wild-type mice at various ages ranging from 3 weeks to 16 months. The results, summarized in Figure 2, revealed reduced cAMP concentrations in striatal 1.5-fold ($P < 0.001$) and cortical extracts 1.2-fold ($P < 0.001$), compared with wild-type littermate extracts, that manifest between 6 and 10 weeks of age, worsening thereafter. By contrast, cAMP levels in mutant and wild-type cerebellar extracts were similar even at 16 months. Therefore, the decline in cAMP was progressive and selectively manifest in Hdh^{Q111} striatum, and cerebral cortex, as expected for a consequence of mutant huntingtin that may be involved in the disease process in man.

Reduced cAMP in HD lymphoblasts and postmortem HD brain

To test this possibility directly, we used EIA to determine cAMP concentrations in HD patient and non-HD control postmortem brain and lymphoblastoid cell extracts. The results are summarized in the scatter plot shown in Figure 3. For parietal cortex extracts from the three control postmortem brains, the group mean cAMP level was 0.84 ± 0.21 pmol/ml (range mean ± SD 0.64 ± 0.11 to 0.97 ± 0.31 pmol/ml). By contrast, the extracts from five age-matched HD postmortem brains (Vonsattel neuropathologic grade 3) exhibited a group mean cAMP level of 0.29 ± 0.07 pmol/ml (range mean ± SD 0.22 ± 0.06 to 0.39 ± 0.11 pmol/ml), disclosing a striking 2.8-fold reduction ($P < 0.001$). Similarly, HD and control lymphoblastoid cell extracts exhibited group mean cAMP levels of 0.30 ± 0.09 pmol/ml (range mean ± SD 0.28 ± 0.01 to 0.31 ± 0.16 pmol/ml) and 0.61 ± 0.15 pmol/ml (range mean ± SD 0.55 ± 0.07 to 0.67 ± 0.22 pmol/ml), respectively, revealing a significant ~2.1-fold decrease ($P < 0.005$). Thus, decreased cAMP reflects a dominant disease process that is manifest in non-neuronal as well as brain cells from HD patients.

$STHdh^{Q111}$ striatal cells exhibit decreased PKA–CREB signaling

We then investigated the basis of decreased cAMP and CRE signaling, using striatal neuronal cell lines generated from homozygous and heterozygous Hdh^{Q111} and wild-type Hdh^{Q7} littermate embryos (5). First, immunoblot analyses confirmed decreased CRE signaling in mutant $STHdh^{Q111}$ cells, compared with wild-type striatal cells. BDNF signal was decreased (data not shown) (20) and, as shown in Figure 4A, phospho-CREB signal was reduced by ~1.3-fold. To determine whether decreased cAMP–PKA signaling might involve altered CBP, CBP complexes were immunoprecipitated from cytosolic and

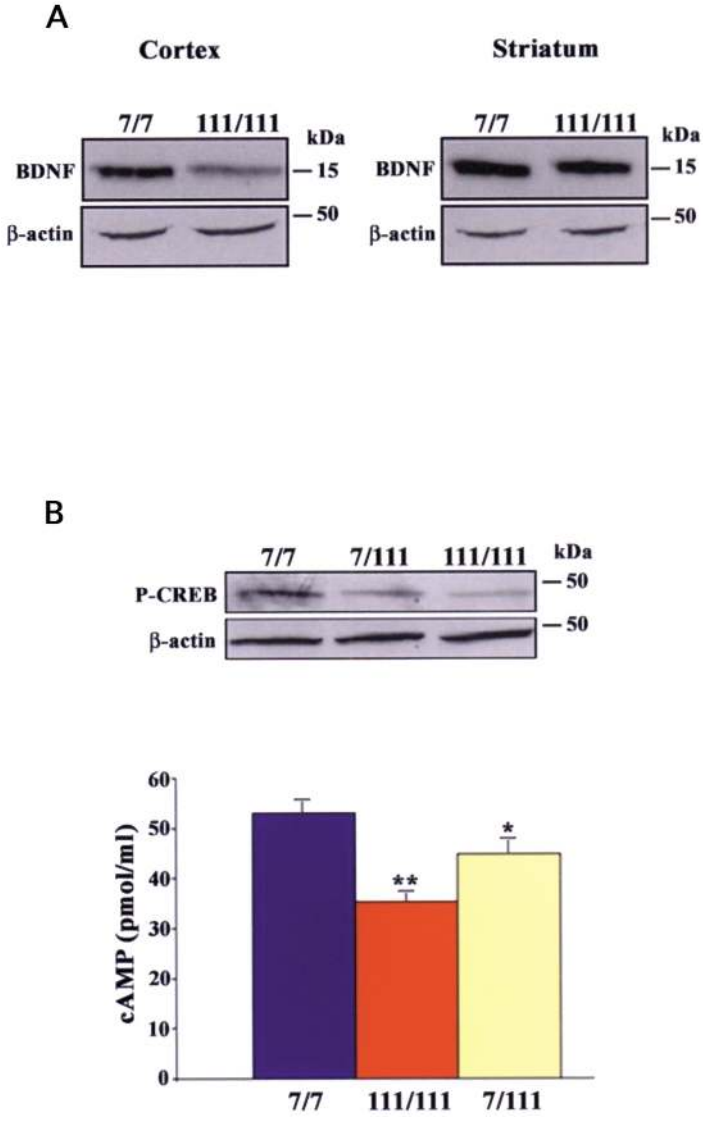

Figure 1. Reduced PKA-signaling and cAMP in Hdh^{Q111} striatum and cortex (**A**) Immunoblot showing decreased BDNF band intensity at 5 months of age in Hdh^{Q111} homozygote (111/111) compared with wild-type (7/7) littermate cerebral cortical (cortex) and striatal (striatum) extracts. Densitometry revealed a 2.2-fold decrease in mutant cortex BDNF: β-actin band intensity ratios (wild-type 0.81/0.80 units; mutant 0.41/0.90 units) and a 1.4-fold decrease for mutant striatum (wild-type 1.12/0.57 units; mutant 0.90/0.64 units). (**B**) Top: immunoblot showing decreased phospho-CREB band intensity at 5 months of age in Hdh^{Q111} homozygote (111/111) and Hdh^{Q111} heterozygote (7/111) compared with wild-type (7/7) littermate cerebral cortex (cortex) extracts. Phospho-CREB: β-actin band intensity ratios for wild-type (8.25/2.89), heterozygous mutant (3.68/3.10) and homozygous mutant (1.42/3.36), revealed decreases of 2.2- and 4.5-fold, respectively. Bottom: histogram displaying reduced cAMP concentration measured by EIA in extracts from cerebral cortex from Hdh^{Q111} homozygotes (111/111) and heterozygotes (7/111) compared with wild-type (7/7) littermates at 5 months of age. Values are the mean ± SD of quadruplicate determinations. Statistical significance, $*P < 0.05$; $**P < 0.001$.

nuclear fractions of wild-type $STHdh^{Q7}$ and homozygous $STHdh^{Q111}$ cells. As shown in the immunoblot in Figure 4B, the CBP reagent detected a nuclear CBP band in precipitates from wild-type and mutant cells, although in the latter cytoplasmic CBP was also detected. Confocal immunostaining of wild-type and heterozygous and homozygous mutant striatal cells, in Figure 4C, confirmed a nuclear pattern of CBP-stain in wild-type cells. By contrast, the majority of heterozygous and homozygous mutant cells exhibited both perinuclear and nuclear CBP stain, indicating that perinuclear CBP was a dominant effect of mutant huntingtin. Quantification (Fig. 4D) revealed CBP signal confined to the nucleus in 100% of wild-type cells but only in ~18% of homozygous mutant cells.

Since mutant striatal cells do not display accumulated mutant amino terminal huntingtin inclusions (5), CBP sequestration seemed unlikely to explain perinuclear CBP in mutant cells. Therefore, to determine whether this distinct distribution might instead be dynamic and reflect altered cAMP–PKA signaling, wild-type and homozygous mutant cells were treated with forskolin. As shown in Figure 4D, forskolin restored a wild-type nuclear CBP pattern in the majority (88%) of mutant striatal cells. Thus, perinuclear CBP in mutant striatal cells

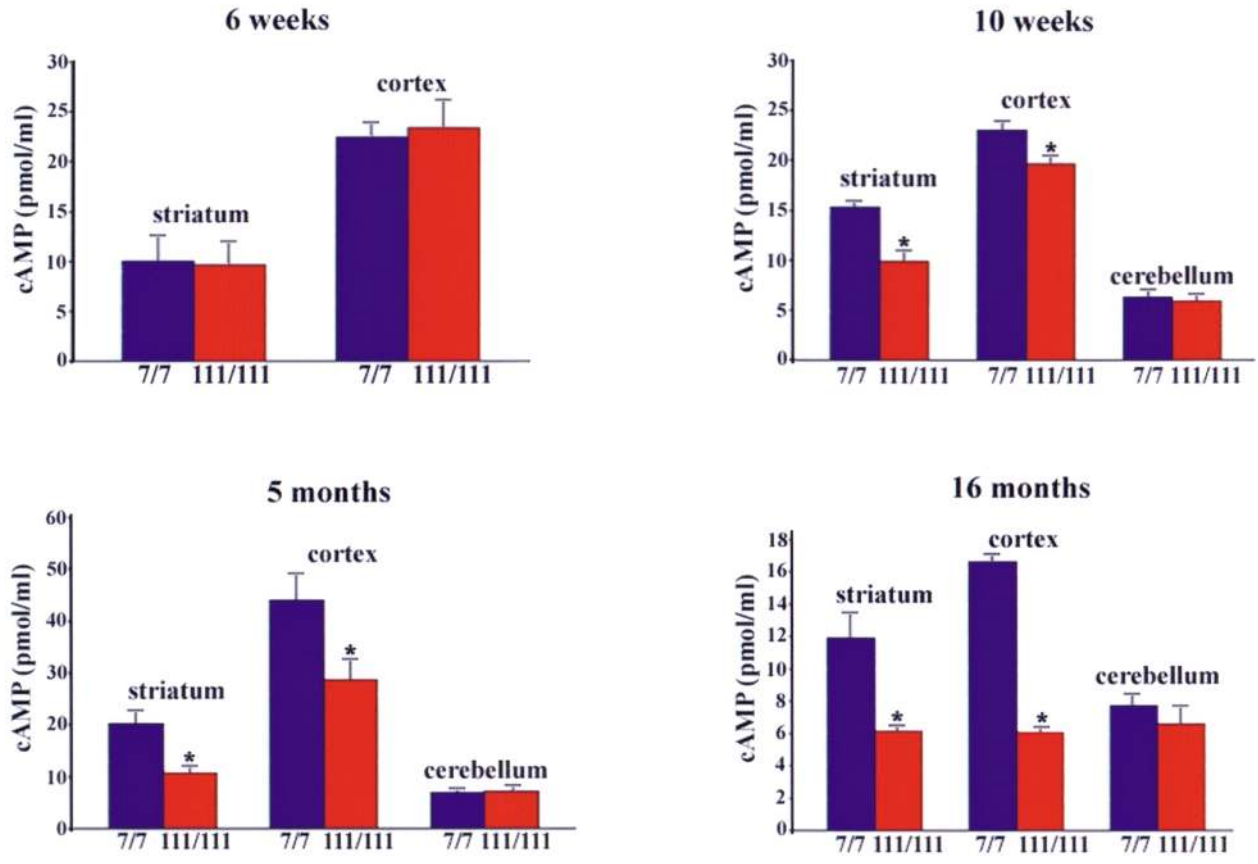

Figure 2. Timing and regional selectivity of reduced cAMP in Hdh^{Q111} brain. Histogram to show cAMP levels measured in extracts from Hdh^{Q111} homozygote (111/111) and wild-type (7/7) striatum, cerebral cortex and cerebellum at ages from 6 weeks to 16 months. Measurement at 3 weeks disclosed no difference between mutant and wild-type in these regions (data not shown). Values are the mean ± SD of quadruplicate determinations. Statistical significance, $*P < 0.001$.

appears to be due to decreased cAMP–PKA signaling, implying reduced cAMP as a consequence of mutant huntingtin.

STHdh^{Q111} striatal cells exhibit decreased cAMP synthesis

Therefore, we measured cAMP in extracts of wild-type *STHdh*^{Q7} and mutant *STHdh*^{Q111} cells. The results of EIA cAMP assays, in Figure 5A, disclosed significantly decreased cAMP levels in homozygous and heterozygous *STHdh*^{Q111} cell extracts, of 1.7-fold ($P < 0.001$) and 1.4-fold ($P < 0.005$), respectively, compared with wild-type levels. Moreover, when adenylyl cyclase activity was stimulated by addition of forskolin to the growth medium, cAMP concentration was increased for all genotypes, but levels in extracts from homozygous and heterozygous cells remained lower than wild-type by 1.5-fold ($P < 0.001$) and 1.2-fold ($P < 0.05$), respectively (Fig. 5A). As these data suggested dominantly altered cAMP synthesis or degradation, we determined cAMP levels in extracts of homozygous *STHdh*^{Q111} cells and *STHdh*^{Q7} cells as a function of time after forskolin treatment. The results, in Figure 5B, revealed a shallower slope and cAMP maximum for mutant cells that was approximately two-thirds that achieved in wild-type striatal cells. This discrepancy was not eliminated by the addition of the phosphodiesterase inhibitor Ro-201724, although basal and forskolin-induced cAMP levels were elevated (data not shown), demonstrating that differential degradation was unlikely to explain restricted cAMP levels observed in mutant striatal cell extracts.

STHdh^{Q111} striatal cells display reduced ATP and ATP/ADP ratio

We measured ATP, the substrate for adenylyl cyclases, using an assay based on firefly luciferase activity, for which ATP is an essential and specific co-factor. As shown in Figure 6A, compared with wild-type extract, homozygous and heterozygous *STHdh*^{Q111} cell extracts exhibited a significant reduction in ATP, of 2.2-fold ($P < 0.001$) and 1.4-fold ($P < 0.001$), respectively, disclosing decreased ATP as a dominant consequence of mutant huntingtin.

To determine whether reduced ATP might reflect a deficit in energy metabolism, the relative levels of adenosine nucleotides were measured by HPLC in equivalent protein extracts prepared from *STHdh*^{Q7} and homozygous *STHdh*^{Q111} cells. Typical HPLC profiles, in Figure 6B, and calculated summary data, in Figure 6C, disclosed a relative reduction in cAMP, as well as ATP, but an increase in ADP in mutant cell extracts. The ratio of ATP/ADP, a measure of mitochondrial energy function,

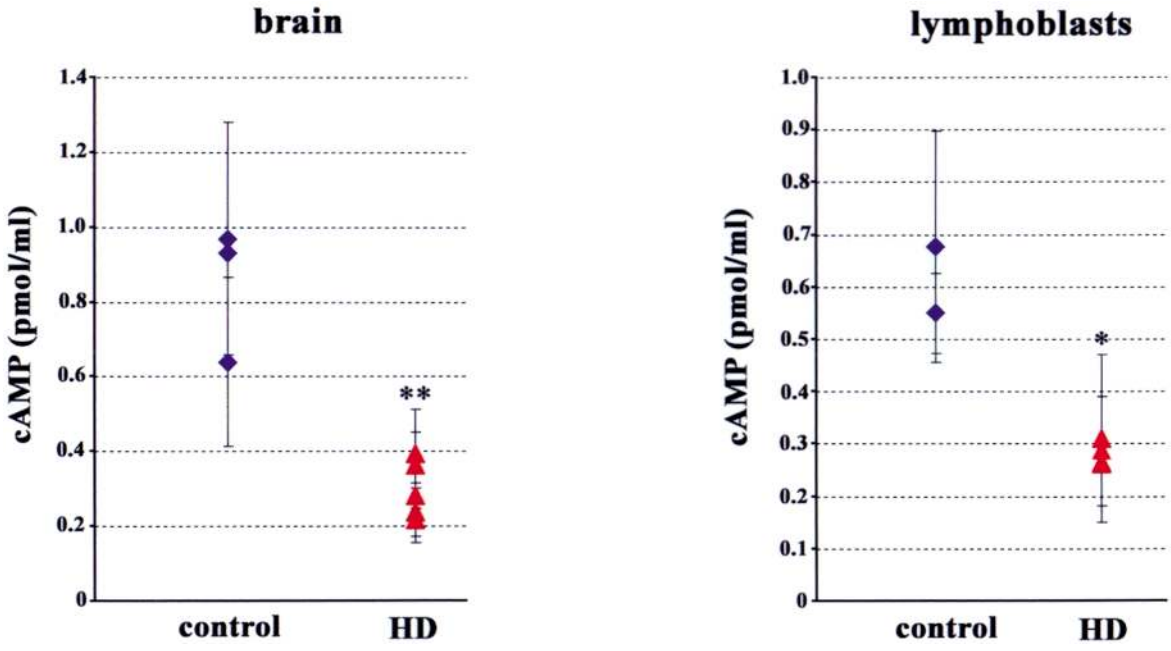

Figure 3. Decreased cAMP levels in HD brain and lymphoblastoid cells. Left: scatter plot displaying cAMP concentration detected in extracts of parietal cortex dissected from 3 non-HD (control) and five age-matched HD (HD) postmortem brains. Controls: *HD* CAG repeats of 25/17, 21/21 and 20/18 units yielded mean cAMP levels of 0.97, 0.64 and 0.93 pmol/ml, respectively. HD: *HD* CAG repeats of 41/18, 41/37, 42/32, 43/17 and 43/17 units yielded mean cAMP levels of 0.36, 0.28, 0.23, 0.39, and 0.22 pmol/ml, respectively. Right: scatter plot of cAMP concentration detected in extracts of lymphoblastoid cells established from two normal individuals (control) and three HD patients (HD). Controls: *HD* CAG repeats of 18/17 and 17/15 units yielded mean cAMP levels of 0.67 and 0.55 pmol/ml, respectively. HD: *HD* CAG repeats of 39/17, 56/21 and 52/18 units yielded mean cAMP levels of 0.28, 0.28 and 0.30 pmol/ml, respectively. Values are the mean ± SD of triplicate determinations. Statistical significance, $*P < 0.005$; $**P < 0.001$.

is plotted in Figure 6D, indicating a significantly reduced ratio in mutant striatal cells ($P < 0.001$), suggesting a respiratory chain defect.

STHdh^{Q111} striatal cells exhibit mitochondrial respiratory chain deficits

We therefore assessed mitochondrial energy metabolism in naive wild-type and homozygous mutant *STHdh*^{Q111} cells, and in cells treated with the oxidative stressor H_2O_2, using the conversion of MTT to formazan to assess the mitochondrial electron transport chain. The results, summarized in Figure 7A, revealed that compared with untreated wild-type cells formazan production was significantly reduced by ~30% in untreated mutant cells ($P < 0.001$). Furthermore, H_2O_2 treatment caused a more dramatic reduction in formazan production in mutant cells compared with wild-type cells (41 and 18%, respectively), consistent with a defect of mitochondrial respiratory chain activity.

To directly test respiratory chain function, we assessed the sensitivity of wild-type *STHdh*^{Q7} and homozygous mutant striatal cells to 3-nitropropionic acid (3-NP), a succinate dehydrogenase inhibitor, by measuring cell survival. DAPI staining revealed nuclear blebbing that was more prominent in treated mutant *STHdh*^{Q111} cells (data not shown). Quantification of all DAPI stained nuclei in treated and parallel mock treated cultures (Fig. 7B) revealed a significant ~2.5-fold decrease ($P < 0.001$) in the survival of 3-NP challenged mutant cells, compared to their wild-type counterparts, consistent with a mitochondrial respiratory chain deficit that reduces cell survival.

DISCUSSION

In HD, the graded loss of vulnerable neurons in the striatum underlies the distinctive clinical symptoms of the disorder. We have tested the hypothesis that the dominant pathogenic process triggered by mutant huntingtin might lead to an early metabolic deficit that amplifies the disease cascade by altering cAMP-dependent processes, including CRE-mediated gene transcription.

Our findings in genetically accurate HD mouse and striatal cell models provide the first evidence that a striatal specific energy deficit, manifest as reduced cAMP and ATP/ADP ratio, is an early, unremitting consequence of mutant huntingtin. Indeed, decreased cAMP is evident in *Hdh*^{Q111} striatum by 10 weeks of age, preceding amino terminal aggregate and intranuclear inclusions by almost a year and predating reactive gliosis and overt neurodegenerative changes by ~2 years. These data, therefore, strongly suggest that selective metabolic impairment precedes neuropathology and clinical symptoms in HD patients. Moreover, consistent with low cAMP in cerebral spinal fluid (25), dramatically reduced cAMP in HD post-mortem brain and lymphoblastoid cells indicates a chronic deficit in HD patients that ultimately involves many cell types.

The precise steps by which mutant huntingtin leads to impaired cAMP and energy metabolism are not known, but may involve a direct interaction of the mutant protein with the

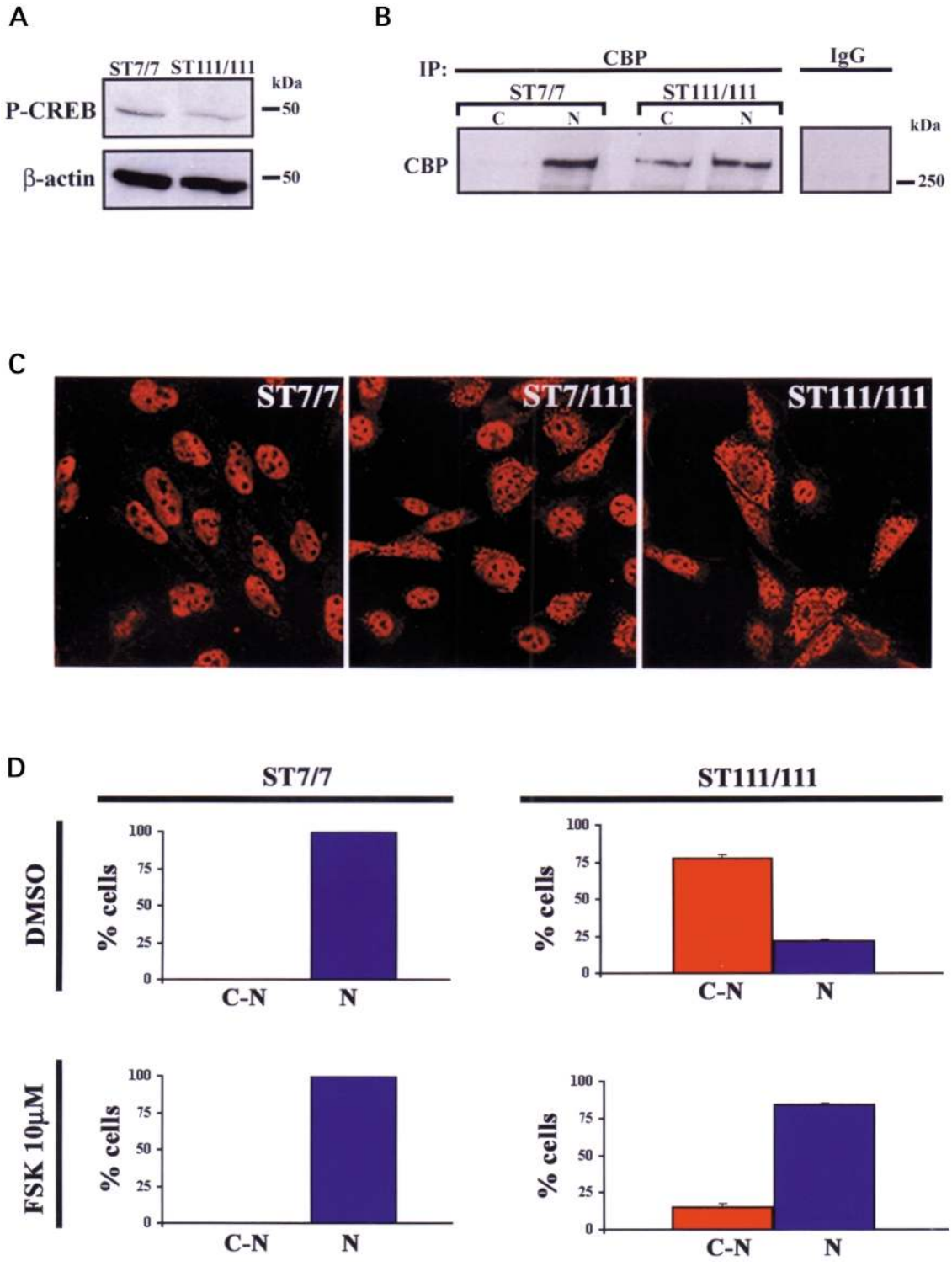

Figure 4. Decreased PKA/CREB signaling in $STHdh^{Q111}$ striatal cells. (**A**) Immunoblot showing phospho-CREB levels in $STHdh^{Q111}/Hdh^{Q111}$ (ST111/111) and wild-type $STHdh^{Q7}/Hdh^{Q7}$ (ST7/7) cell extracts. Phospho-CREB: β-actin band intensity ratios for wild-type (0.27/6.62 units) and homozygous mutant (0.19/6.37 units) revealed a 1.3 fold decrease in mutant compared to wild-type extract. (**B**) Immunoblot analysis of CBP-complexes precipitated from cytosolic and nuclear fractions, showing increased CBP-reactive band in the cytoplasmic fraction of $STHdh^{Q111}/Hdh^{Q111}$ (ST111/111) mutant cells compared with $STHdh^{Q7}/Hdh^{Q7}$ (ST7/7) wild-type striatal cells. Control IgG precipitate is shown. Blot detected with anti-CBP reagent. (**C**) Confocal microscopy revealed dominant perinuclear distribution of CBP in heterozygous $STHdh^{Q7}/Hdh^{Q111}$ (ST7/111) and homozygous $STHdh^{Q111}/Hdh^{Q111}$ (ST111/111) mutant striatal cells. CBP-signal was nuclear in wild-type (ST7/7) cells. (**D**) Histogram showing the proportion of wild-type $STHdh^{Q7}/Hdh^{Q7}$ (ST7/7) and homozygous mutant $STHdh^{Q111}/Hdh^{Q111}$ (ST111/111) striatal cells exhibiting CBP-stain that was cytoplasmic + nuclear (C-N) or only nuclear (N) in cultures treated with DMSO or with forskolin (FSK). All of the wild-type cells ($n = 230$) exhibited CBP signal confined to the nucleus, while an average of 18% of mutant cells (36/201cells) showed this pattern. Activation of cAMP/PKA signaling by forskolin restored a nuclear CBP phenotype in about 88% (132/150 cells) of the mutant striatal cells.

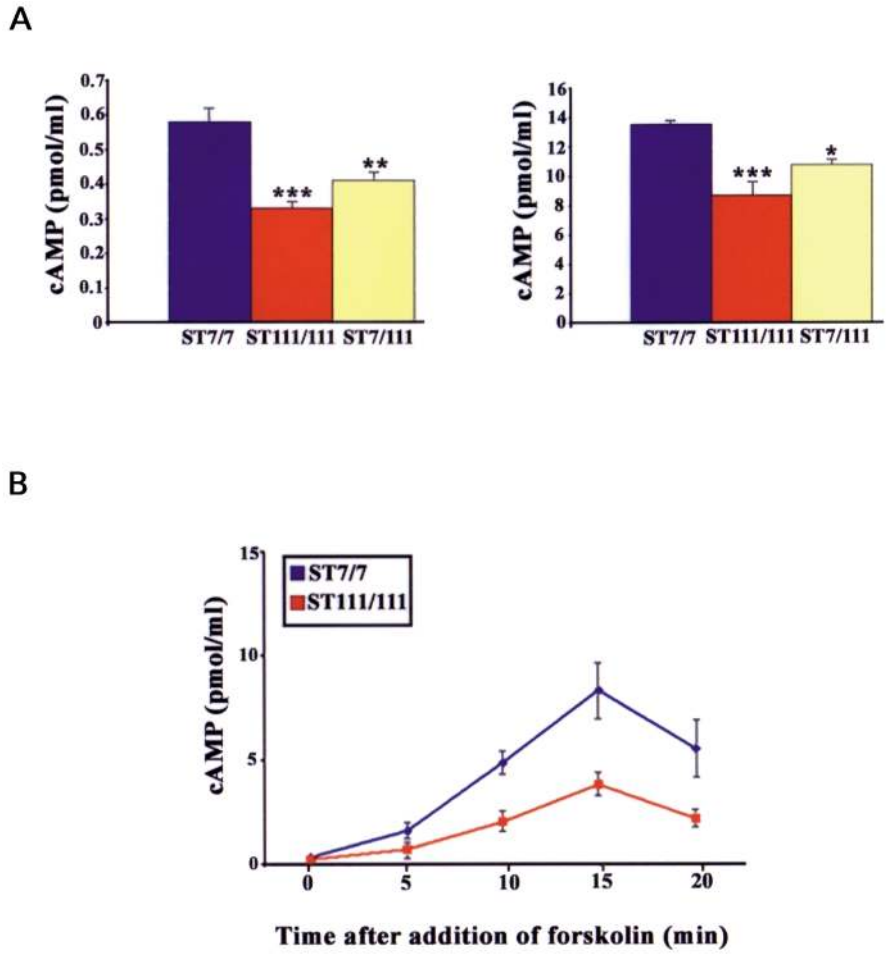

Figure 5. Mutant striatal cells exhibit dominantly decreased cAMP. (**A**) Histogram showing reduced basal (left) and forskolin-induced (right) levels of cAMP in homozygous $STHdh^{Q111}/Hdh^{Q111}$ (ST111/111) and heterozygous $STHdh^{Q111}/Hdh^{Q7}$ (ST7/111) striatal neuronal cell extracts compared to wild-type $STHdh^{Q7}/Hdh^{Q7}$ (ST7/7). Values are the mean ± SD of triplicate determinations. Statistical significance, $*P < 0.01$; $**P < 0.005$; $***P < 0.001$. (**B**) Plot of cAMP concentration versus time displaying similar time course, but limited cAMP induction in homozygous mutant $STHdh^{Q111}/Hdh^{Q111}$ cells (ST111/111) compared to wild-type $STHdh^{Q7}/Hdh^{Q7}$ (ST7/7) striatal cell extracts, after addition of 10 μM of forskolin to growth medium. Values are the mean ± SD of triplicate determinations.

mitochondrion (27). Our results in $STHdh^{Q111}$ cells demonstrate a reduced ATP/ADP ratio that directly implicates a mitochondrial respiratory chain deficit, supported by reduced respiratory chain activity in the MTT assay and the hypersensitivity of mutant striatal cells to mitochondrial toxins. This deficit would be consistent with respiratory complex deficiencies reported in cells from symptomatic HD patients (13).

ATP deficit, which was associated with low cAMP in mutant striatal cells, may underlie declining Hdh^{Q111} striatal cAMP levels *in vivo*. Limiting ATP substrate and/or free radicals produced during oxidative stress would be expected to decrease adenylyl cyclase activity (30), restricting cAMP synthesis. However, it is also possible that reduced ATP may be a consequence of decreased cAMP. The disease process may first lead to a reduction in cAMP, for example via a reduction in the levels of specific adenylyl cyclases (15), with consequent impact on mitochondrial energy function.

Decreased CRE-mediated signaling in Hdh^{Q111} striatal cells appears to be explained by reduced cAMP, which occurs early in the disease cascade in the absence of amino terminal huntingtin inclusions, rather than by transcription factor sequestration or loss of huntingtin pro-survival activity. This finding suggests that low cAMP may give rise to altered CRE-regulated gene transcription observed in HD postmortem brain (20,23) and in transgenic HD mouse and cell culture models (15,19–22).

Energy deficit and decreased CRE-mediated signaling might amplify the disease cascade in multiple ways. Our findings, together with defective NMDA receptor-mediated neuronal cell swelling found in *Hdh*CAG94 knock-in brain (31) and decreased aconitase in R6/2 brain (32), support NMDA receptor mediated excitotoxicity (reviewed in 14) early in the disease process. Moreover, CREB function, which is required to sustain adult CNS neurons (33), mediates nuclear calcium regulated gene transcription following neuronal cell membrane depolarization (34). Furthermore, survival factors, such as BDNF, and a host of other CRE-regulated gene products altered in HD model systems, including DARPP-32, enkephalin and somatostatin, are essential for normal neuronal cell function.

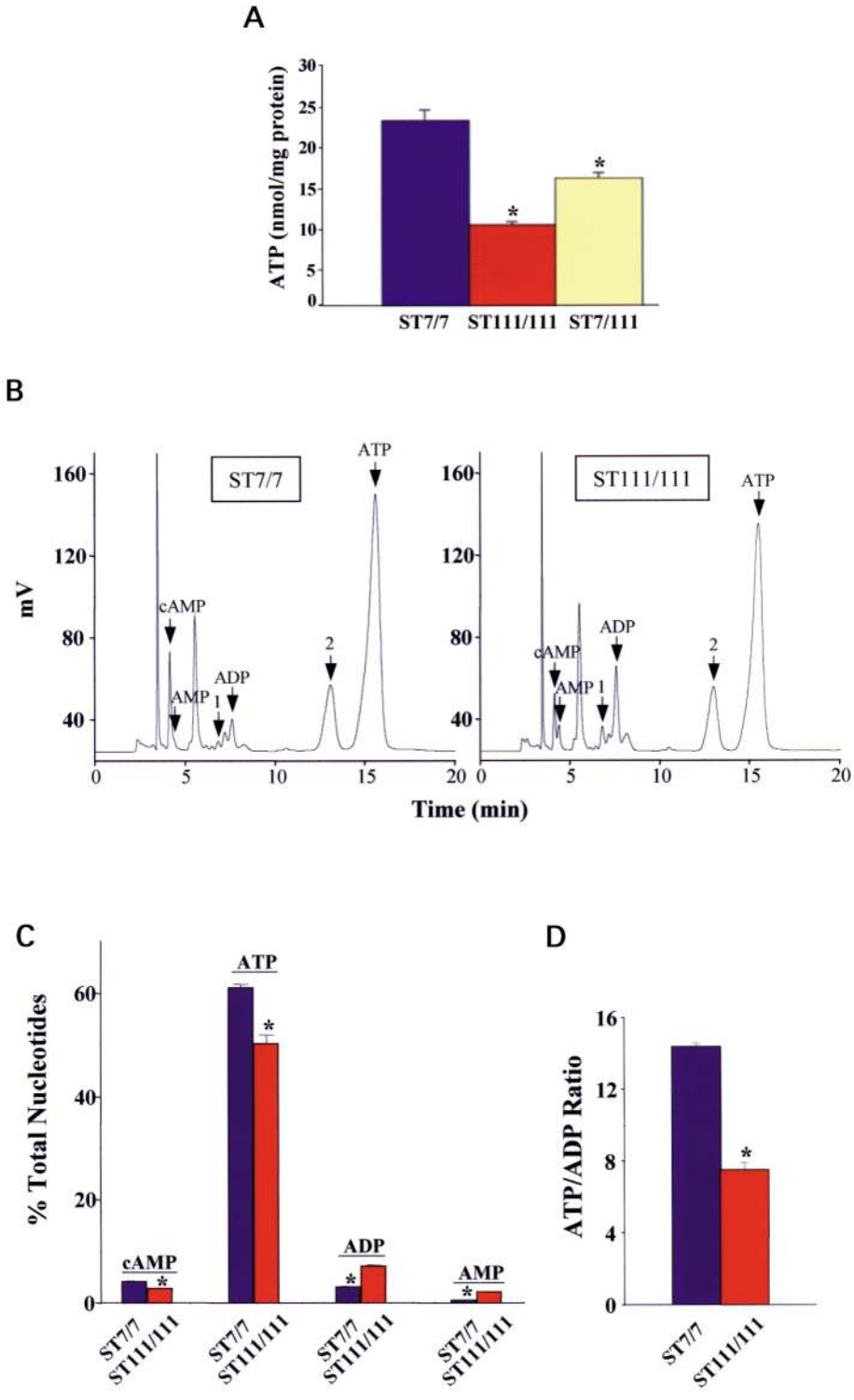

Figure 6. *STHdh*^{Q111} striatal cells exhibit decreased ATP and ATP/ADP ratio. (**A**) Histogram of ATP concentration demonstrating reduced levels in homozygous *STHdh*^{Q111}/*Hdh*^{Q111} (ST111/111) and heterozygous *STHdh*^{Q111}/*Hdh*^{Q7} (ST7/111) striatal neuronal cells extracts compared with wild-type *STHdh*^{Q7}/*Hdh*^{Q7} cells (ST7/7) using luminometric assay. Values are the mean ± SD of triplicate determinations. Statistical significance, *$P < 0.001$. (**B**) HPLC chromatograms showing adenosine nucleotides in wild-type *STHdh*^{Q7}/*Hdh*^{Q7} (ST7/7) and decreased cAMP and ATP, with increased AMP and ADP, in homozygous *STHdh*^{Q111}/*Hdh*^{Q111} (ST111/111) mutant striatal cells. Guanosine nucleotides are also indicated (1 = GDP, 2 = GTP). (**C**) Histogram showing relative amounts of adenosine nucleotides in wild-type *STHdh*^{Q7}/*Hdh*^{Q7} (ST7/7) and homozygous *STHdh*^{Q111}/*Hdh*^{Q111} (ST111/111) mutant striatal cells. Values are the mean ± SD of triplicate determinations. cAMP, ATP, ADP and AMP values are expressed as percentages of the cellular nucleotide pool. Statistical significance, *$P < 0.001$. (**D**) Histogram displaying ATP/ADP ratio in wild-type *STHdh*^{Q7}/*Hdh*^{Q7} (ST7/7) and homozygous *STHdh*^{Q111}/*Hdh*^{Q111} (ST111/111). Values are the mean ± SD of triplicate determinations. Statistical significance, *$P < 0.001$.

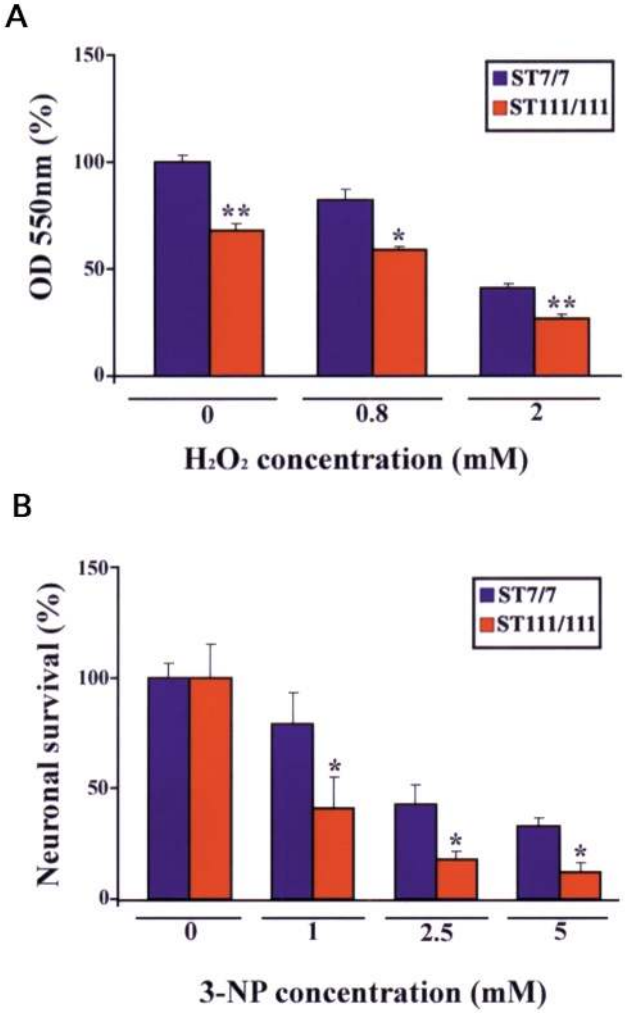

Figure 7. Mutant $STHdh^{Q111}$ striatal cells display mitochondrial deficits. (**A**) Histogram displaying the reduction in MTT conversion in homozygous mutant $STHdh^{Q111}/Hdh^{Q111}$ (ST111/111) and wild-type $STHdh^{Q7}/Hdh^{Q7}$ (ST7/7) striatal cells following H_2O_2 treatment. Statistical significance, $*P < 0.005$; $**P < 0.001$. (**B**) Histogram displaying the decreased proportion of homozygous mutant $STHdh^{Q111}/Hdh^{Q111}$ (ST111/111) and wild-type $STHdh^{Q7}/Hdh^{Q7}$ (ST7/7) striatal cells surviving 3-NP treatment. Statistical significance, $*P < 0.001$.

Notably, cAMP-mediated signaling is integral to mitochondrial function. CREB regulates cytochrome c transcription (35) and cAMP directly modulates mitochondrial membrane potential, respiration and formation of reactive oxygen species (ROS) (36). Thus, our findings support an early disease process in which mutant huntingtin may lead to mitochondrial respiratory chain impairment and reduced cAMP. Consequently decreased CRE-regulated gene transcription may 'feedback', further depressing energy metabolism. This proposal is consistent with the hypothesis that energy impairment in HD neuronal cells may lead to catastrophic ATP deficiency (13). Our data also provide strong evidence that ATP/ADP ratio and cAMP merit investigation as early progressive biochemical markers in HD and suggest that pharmacological manipulation of energy metabolism at an early stage may slow the pathogenic process in HD brain.

MATERIALS AND METHODS

Hdh^{Q111} knock-in mice

Hdh^{Q111} knock-in mice, with targeted insertion of 109 CAG repeats that extends the glutamine segment in murine huntingtin to 111 residues (37), were maintained on a CD1 outbred genetic background (Charles River Laboratories, Wilmington, MA, USA). Hdh^{Q111} heterozygote males and females were intercrossed to produce Hdh^{Q111} heterozygotes and homozygotes and wild-type littermates. Genotyping for CAG repeat size was performed as described (37).

Immortalized $STHdh^{Q111}$ striatal neuronal cell lines

Conditionally immortalized wild-type $STHdh^{Q7}$ striatal neuronal progenitor cells expressing endogenous normal huntingtin, and homozygous and heterozygous mutant $STHdh^{Q111}$ striatal neuronal progenitor cell lines, expressing endogenous mutant huntingtin with 111-glutamines, have been described previously (5). The striatal cell lines were grown at 33°C in Dulbecco's modified Eagle's medium (DMEM) supplemented with 10% fetal bovine serum (FBS), 1% non-essential amino acids, 2 mM L-glutamine and 400 µg/ml G418 (Geneticin; GIBCO-BRL, Life Technologies, Gaithersburg, MD, USA). Cells were treated by addition of agents (Sigma-Aldrich, St Louis, MO, USA) to growth medium: forskolin (10 µM) for 30 min, with or without Ro 20-1724 [4-(3-butoxy-4-methoxybenzyl)-2-imidazolidinone; 0.5 mM], or with 3-nitropropionic acid. Cell survival was determined with striatal cells plated on tissue culture 'welled' glass slides (Becton Dickinson, Franklin Lakes, NJ, USA) at density of 1.5×10^5/well (triplicate wells). Twenty-four hours later fresh growth medium without (control) or with 3-nitropropionic acid (1, 2.5 or 5 mM) was added. After 3 days the cells were rinsed, fixed for 15 min in 4% paraformaldehide, permeabilized with 0.1% Triton-X100 for 5 min and incubated with DAPI (0.5 µg/ml, Molecular Probes, Eugene, OR, USA) for 5 min. DAPI-stained nuclei were counted ($n = 3$ independent experiments) using confocal microscope (MRC-1024 laser confocal microscope, BioRad, Hercules, CA, USA). Survival represents the proportion of nuclei counted in treated wells relative to nuclei counted in parallel untreated wells (100%).

Postmortem brain tissue and lymphoblastoid cell lines

The Harvard Brain Tissue Resource Center, McLean Hospital (Belmont, MA, USA) supplied the postmortem brain tissue. Three control (non-HD) cases, which had postmortem intervals of 2–32 h were from two males and one female (mean age 76 years). Cause of death was listed as myocardial infarct. Five HD cases (HD neuropathology Vonsattel grade 3) had postmortem intervals of 8–30 h and were from five males (mean age 70 years), with death at end-stage disease. The HD CAG allele sizes were determined previously: control brain 25/17, 21/21, 20/18; HD brain 41/18, 41/37, 42/23, 43/17. Tissue was used pursuant to the guidelines of the MGH IRB for

discarded human tissue. Previously genotyped lymphoblastoid cell lines from two control non-HD individuals (HD CAG repeats; 17/18, 17/15 units) and three HD patients (39/17; 56/21; 52/18 units) have been described (1,38).

Subcellular fractionation and immunoprecipitation

Wild-type $STHdh^{Q7}/Hdh^{Q7}$ and homozygous mutant $STHdh^{Q111}/Hdh^{Q111}$ cells were harvested and cell pellets used to prepare cytosolic and nuclear fractions. The cell pellet was suspended in buffer A [10 mM Hepes (pH 7.9) containing 1.5 mM $MgCl_2$, 10 mM KCl, protease inhibitor cocktail and 1 mM PMSF] left on ice for 10 min, subjected to homogenization by 40 strokes in a Douncer homogenizer and centrifuged at 2000*g* for 15 min. The supernatant was collected for provide the cytosolic fraction. The pelleted fraction was resuspended in buffer C [20 mM Hepes (pH 7.9) containing 25% glycerol, 0.42 M KCl, 1.5 mM $MgCl_2$, 0.2 mM EDTA, protease inhibitor cocktail and 1 mM PMSF] with gentle rotation (30 min at 4°C). The mixture was centrifuged at 12 000*g* for 10 min to yield the nuclear fraction The protein content of each fraction was determined using Bio-Rad DC (Detergent Compatible) protein assay (Bio-Rad, Hercules, CA, USA).

Immunoprecipitation was done by incubation (overnight at 4°C) of nuclear and cytosolic cell fractions (500 µg) with 3 µg of anti-CBP-A22 antibody (Santa Cruz Biotechnology, Santa Cruz, CA, USA). The complexes were then incubated for further 2 h with protein A Sepharose CL-4B (Sigma) with gentle rotation. The immunocomplexes were then washed by centrifugation and resuspension two times in 1% NP-40 buffer and once in PBS. After boiling for 5 min in reducing SDS sample buffer the immunoprecipitated proteins were resolved by SDS–PAGE on 6% polyacrylamide gel and transferred to nitrocellulose membranes. Immunoprecipitate complexes were detected by incubation with anti-CBP antibody followed by HRP-conjugated secondary antibody and enhanced chemiluminescence as described above.

Immunoblot analyses

Protein extracts of cerebral cortex and striatum dissected from Hdh^{Q111} and wild-type mice (5 months age) were produced by lysis of minced tissue in ice-cold buffer (50 mM Tris–HCl pH 7.4–150 mM NaCl–2 mM EDTA–1% NP-40–1 mM PMSF). The supernatant was recovered after centrifugation at 10 000*g*. Protein extracts (30 µg) were resolved on 10 and 15% SDS–PAGE, proteins were transferred to nitrocellulose membranes (Schleicher & Schuell), blocked with 10% non-fat milk and incubated with primary antibodies overnight at 4°C and detected by horseradish peroxidase-conjugated secondary antibody-enhanced chemiluminescence (ECL) reagents (New England Biolabs, Beverly, MA, USA). Phosphoimager analyses were used to quantify the intensity of BDNF and phospho-CREB relative to the intensity of the β-actin band in the same lane. Antibody reagents were anti-BDNF (Santa Cruz Biotechnology, Santa Cruz, CA, USA), anti-phospho-CREB Ser133 (Cell Signaling, Beverly, MA, USA) and anti β-actin (Sigma-Aldrich, St Louis, MO, USA).

Immunofluorescence and confocal analysis

Wild-type $STHdh^{Q7}/Hdh^{Q7}$ and homozygous mutant $STHdh^{Q111}/Hdh^{Q111}$ cells were grown on four chambers glass slides (Becton Dickinson, Franklin Lakes, NJ, USA) at a density of 6×10^5/well (duplicate wells). The cells were fixed in 4% paraformaldehide, permeabilized for 5 min in 0.1% Triton X-100 in PBS treated for 30 min in blocking buffer (1% bovine serum albumin in PBS) and incubated for 2 h in blocking solution containing anti-CBP-A22. After several washes in PBS (3×5 min), cells were then incubated for 1 h in blocking solution containing goat anti-rabbit Cy3 secondary antibody (Jackson ImmunoResearch, West Grove, PA, USA). Cells were imaged with a laser confocal microscope (Bio Rad, Hercules, CA, USA) using the 20× objective.

cAMP competitive enzyme immunoassay

cAMP measurements were performed using the Direct cAMP enzyme immunoassay (EIA) kit CA-200 (Sigma-Aldrich, St Louis, MO, USA), according to the protocol supplied by the manufacturer. Frozen dissected mouse or human brain tissue was lysed directly in 0.1 M HCl (20 min) and supernatant recovered after centrifugation at 9000*g*. Dissected Hdh^{Q7} and Hdh^{Q111} knock-in mouse tissue was pooled: 6 weeks ($n = 2$) 10 weeks ($n = 3$); 5 months ($n = 4$); and 16 months of age ($n = 3$). For cultured cells, PBS washed pellets were lysed in 0.1 M HCl (10 min) and supernatant recovered after centrifugation at 2000*g*. An aliquot of cleared lysate was used to determine protein concentration using Bio-Rad DC (Detergent Compatible) protein assay (Bio-Rad, Hercules, CA, USA). EIA was performed with equal protein. Each EIA determination represents the mean of values obtained with quadruplicate (brain) or triplicate (cells) protein aliquots. cAMP concentration (pmol/ml) was determined by interpolation to a curve produced in the same assay with known concentrations of cAMP (standard curve) supplied by the manufacturer.

Measurement of ATP

ATP was determined luminometrically (MicroLumat LB96P) using the CytoLux L001-100 kit (PerkinElmer Life Sciences Inc., Boston, MA, USA) to measure light-emitting luciferase-catalyzed oxidation of luciferin, according to the manufacturer. PBS-washed cell pellets were lysed in non-ionic detergent buffer (Perkin-Elmer) for 5 min, lysates were cleared by centrifugation at 2000*g* and an aliquot of the supernatant was used for protein determination using Bio-Rad DC (Detergent Compatible) protein assay (Bio-Rad, Hercules, CA, USA). ATP determinations were performed with equal protein. Each ATP determination represents the mean of values obtained with triplicate aliquots. ATP concentration (nmol of ATP per mg of total protein) was calculated by interpolation to values (triplicates) determined with known concentrations of ATP (standard curve) in the same assay. The ATP standard was provided by the manufacturer.

Nucleotide extraction and HPLC analysis

HPLC analysis was performed on wild-type $STHdh^{Q7}/Hdh^{Q7}$ and homozygous mutant $STHdh^{Q111}/Hdh^{Q111}$ cells to analyze quantitative differences on cellular nucleotide pools. One million cells were pelleted at 800*g* and the pellets washed twice in ice-cold PBS (pH 7.4). Nucleotide extraction was done with 50 µl of ice-cold acetonitrile followed by 150 µl of cold water (39). The soluble and precipitated fractions were centrifuged at 14 000*g* for 10 min at −20°C and the supernatant fraction, kept on ice, was then gassed with N_2 for 15 min to evaporate acetonitrile. The pellet was solubilized with 1 N NaOH, and the protein content was analyzed by Bio-Rad DC protein assay. The column used to perform the HPLC analysis was a 4 µm Nova-Pack C_{18} cartridge (100 × 8 mm inner diameter) equipped with a radial compression chamber (Waters, Milford, MA, USA). The buffer consisted of 20% acetonitrile, 10 mM ammonium phosphate, and 2 mM PIC-A ion-pairing reagent (Waters) and was run isocratically at 1 ml/min (40). Waters HPLC model 510 was used (Waters, Milford, MA, USA), and the ultraviolet (UV) detector model 440 (Waters) was set at 254 nm. HPLC-grade nucleotide standards were used to calibrate the signals. Internal standards were occasionally added to the samples to test recovery, which exceeded 90% for all nucleotides. All data were quantified by Millenium32 Chromatography Manager (Waters) software.

MTT assay

The metabolic activity of mitochondria was estimated by using MTT assay. This method is based on the reduction of the soluble yellow MTT tetrazolium salt to blue insoluble MTT formazan product by mitochondrial succinic dehydrogenase. After treatment with H_2O_2 (0.8 or 2 mM, 2 h) the cells were washed twice with PBS and the MTT (0.5 mg/ml in PBS) was added to each well and incubated for 2 h at 33°C. The medium was carefully removed and 200 µl of acidified isopropyl alcohol was added to solubilize the colored formazan product. Absorbance was read at 550 nm on a multiwell spectophotometer (Molecular Devices).

Statistical analysis

All values are expressed as mean ± SD. Statitical significance was determined by one-way analysis of variance (ANOVA) and Scheffe's *S* post-test for comparisons between multiple groups.

ACKNOWLEDGEMENTS

We thank Drs R. Shapiro and J. Jenkins for assistance with HPLC and M. Anderson, P. Crawford and F. Puglisi in the MGH Genomics Core Facility for tissue culture. This work was supported by NINDS grants NS32765 and NS16367 (HD Center Without Walls), an Anonymous Donor, and the Huntington's Disease Society of America (Coalition for the Cure). S.G. is a recipient of a fellowship from the Huntington's Disease Society of America.

REFERENCES

1. The Huntington's Disease Collaborative Research Group (1993) A novel gene containing a trinucleotide repeat that is expanded and unstable on Huntington's disease chromosomes. *Cell*, **72**, 971–983.
2. Faber, P.W., Barnes, G.T., Srinidhi, J., Chen, J., Gusella, J.F. and MacDonald, M.E. (1998) Huntingtin interacts with a family of WW domain proteins. *Hum. Mol. Genet.*, **7**, 1463–1474.
3. Boutell, J.M., Thomas, P., Neal, J.W., Weston, V.J., Duce, J., Harper, P.S. and Jones, A.L. (1999) Aberrant interactions of transcriptional repressor proteins with the Huntington's disease gene product, huntingtin. *Hum. Mol. Genet.*, **8**, 1647–1655.
4. Hilditch-Maguire, P., Trettel, F., Passani, L.A., Auerbach, A., Persichetti, F. and MacDonald, M.E. (2000) Huntingtin: an iron-regulated protein essential for normal nuclear and perinuclear organelles. *Hum. Mol. Genet.*, **9**, 2789–2797.
5. Trettel, F., Rigamonti, D., Hilditch-Maguire, P., Wheeler, V.C., Sharp, A.H., Persichetti, F., Cattaneo, E. and MacDonald, M.E. (2000) Dominant phenotypes produced by the HD mutation in $STHdh^{Q111}$ striatal cells. *Hum. Mol. Genet.*, **9**, 2799–2809.
6. Colomer, V., Engelender, S., Sharp, A.H., Duan, K., Cooper, J.K., Lanahan, A., Lyford, G., Worley, P. and Ross, C.A. (1997) Huntingtin-associated protein 1 (HAP1) binds to a Trio-like polypeptide, with a rac1 guanine nucleotide exchange factor domain. *Hum. Mol. Genet.*, **6**, 1519–1525.
7. Velier, J., Kim, M., Schwarz, C., Kim, T.W., Sapp, E., Chase, K., Aronin, N. and DiFiglia, M. (1998) Wild-type and mutant huntingtins function in vesicle trafficking in the secretory and endocytic pathways. *Exp. Neurol.*, **152**, 34–40.
8. Kim, M., Velier, J., Chase, K., Laforet, G., Kalchman, M.A., Hayden, M.R., Won, L., Heller, A., Aronin, N. and Difiglia, M. (1999) Forskolin and dopamine D1 receptor activation increase huntingtin's association with endosomes in immortalized neuronal cells of striatal origin. *Neuroscience*, **89**, 1159–1167.
9. Waelter, S., Scherzinger, E., Hasenbank, R., Nordhoff, E., Lurz, R., Goehler, H., Gauss, C., Sathasivam, K., Bates, G.P., Lehrach, H. *et al.* (2001) The huntingtin interacting protein HIP1 is a clathrin and alpha-adaptin-binding protein involved in receptor-mediated endocytosis. *Hum. Mol. Genet.*, **10**, 1807–1817.
10. Modregger, J., DiProspero, N.A., Charles, V., Tagle, D.A. and Plomann, M. (2002) PACSIN 1 interacts with huntingtin and is absent from synaptic varicosities in presymptomatic Huntington's disease brains. *Hum. Mol. Genet.*, **11**, 2547–2558.
11. White, J.K., Auerbach, W., Duyao, M.P., Vonsattel, J.P., Gusella, J.F., Joyner, A.L. and ME., M. (1997) Huntingtin is required for neurogenesis and is not impaired by the Huntington's disease CAG expansion. *Nat. Genet.*, **17**, 404–410.
12. Gusella, J.F. and MacDonald, M.E. (2000) Molecular genetics: unmasking polyglutamine triggers in neurodegenerative disease. *Nat. Rev. Neurosci.*, **1**, 109–115.
13. Tabrizi, S.J., Cleeter, M.W., Xuereb, J., Taanman, J.W., Cooper, J.M. and Schapira, A.H. (1999) Biochemical abnormalities and excitotoxicity in Huntington's disease brain. *Ann. Neurol.*, **45**, 25–32.
14. Grunewald, T. and Beal, M.F. (1999) Bioenergetics in Huntington's disease. *Ann. NY Acad. Sci.*, **893**, 203–213.
15. Luthi-Carter, R., Strand, A., Peters, N.L., Solano, S.M., Hollingsworth, Z.R., Menon, A.S., Frey, A.S., Spektor, B.S., Penney, E.B., Schilling, G. *et al.* (2000) Decreased expression of striatal signaling genes in a mouse model of Huntington's disease. *Hum. Mol. Genet.*, **9**, 1259–1271.
16. Steffan, J.S., Kazantsev, A., Spasic-Boskovic, O., Greenwald, M., Zhu, Y.Z., Gohler, H., Wanker, E.E., Bates, G.P., Housman, D.E. and Thompson, L.M. (2000) The Huntington's disease protein interacts with p53 and CREB-binding protein and represses transcription. *Proc. Natl Acad. Sci. USA*, **97**, 6763–6768.
17. Shimohata, T., Nakajima, T., Yamada, M., Uchida, C., Onodera, O., Naruse, S., Kimura, T., Koide, R., Nozaki, K., Sano, Y. *et al.* (2000) Expanded polyglutamine stretches interact with TAFII130, interfering with CREB-dependent transcription. *Nat. Genet.*, **26**, 29–36.
18. Nucifora, F.C., Jr., Sasaki, M., Peters, M.F., Huang, H., Cooper, J.K., Yamada, M., Takahashi, H., Tsuji, S., Troncoso, J., Dawson, V.L. *et al.* (2001) Interference by huntingtin and atrophin-1 with cbp-mediated transcription leading to cellular toxicity. *Science*, **291**, 2423–2428.

19. Wyttenbach, A., Swartz, J., Kita, H., Thykjaer, T., Carmichael, J., Bradley, J., Brown, R., Maxwell, M., Schapira, A., Orntoft, T.F. *et al.* (2001) Polyglutamine expansions cause decreased CRE-mediated transcription and early gene expression changes prior to cell death in an inducible cell model of Huntington's disease. *Hum. Mol. Genet.*, **10**, 1829–1845.
20. Zuccato, C., Ciammola, A., Rigamonti, D., Leavitt, B.R., Goffredo, D., Conti, L., MacDonald, M.E., Friedlander, R.M., Silani, V., Hayden, M.R. *et al.* (2001) Loss of huntingtin-mediated BDNF gene transcription in Huntington's disease. *Science*, **293**, 493–498.
21. Bibb, J.A., Yan, Z., Svenningsson, P., Snyder, G.L., Pieribone, V.A., Horiuchi, A., Nairn, A.C., Messer, A. and Greengard, P. (2000) Severe deficiencies in dopamine signaling in presymptomatic Huntington's disease mice. *Proc. Natl Acad. Sci. USA*, **97**, 6809–6814.
22. Sipione, S., Rigamonti, D., Valenza, M., Zuccato, C., Conti, L., Pritchard, J., Kooperberg, C., Olson, J.M. and Cattaneo, E. (2002) Early transcriptional profiles in huntingtin-inducible striatal cells by microarray analyses. *Hum. Mol. Genet.*, **11**, 1953–1965.
23. Dunah, A.W., Jeong, H., Griffin, A., Kim, Y.M., Standaert, D.G., Hersch, S.M., Mouradian, M.M., Young, A.B., Tanese, N. and Krainc, D. (2002) Sp1 and TAFII130 transcriptional activity disrupted in early Huntington's disease. *Science*, **296**, 2238–2243.
24. McCampbell, A., Taylor, J.P., Taye, A.A., Robitschek, J., Li, M., Walcott, J., Merry, D., Chai, Y., Paulson, H., Sobue, G. *et al.* (2000) CREB-binding protein sequestration by expanded polyglutamine. *Hum. Mol. Genet.*, **9**, 2197–2202.
25. Cramer, H., Warter, J.M. and Renaud, B. (1984) Analysis of neurotransmitter metabolites and adenosine 3′,5′-monophosphate in the CSF of patients with extrapyramidal motor disorders. *Adv. Neurol.*, **40**, 431–435.
26. Sawa, A., Wiegand, G.W., Cooper, J., Margolis, R.L., Sharp, A.H., Lawler, J.F., Jr., Greenamyre, J.T., Snyder, S.H. and Ross, C.A. (1999) Increased apoptosis of Huntington disease lymphoblasts associated with repeat length-dependent mitochondrial depolarization. *Nat. Med.*, **5**, 1194–1198.
27. Panov, A.V., Gutekunst, C.A., Leavitt, B.R., Hayden, M.R., Burke, J.R., Strittmatter, W.J. and Greenamyre, J.T. (2002) Early mitochondrial calcium defects in Huntington's disease are a direct effect of polyglutamines. *Nat. Neurosci.*, **5**, 731–736.
28. Wheeler, V.C., White, J.K., Gutekunst, C.A., Vrbanac, V., Weaver, M., Li, X.J., Li, S.H., Yi, H., Vonsattel, J.P., Gusella, J.F. *et al.* (2000) Long glutamine tracts cause nuclear localization of a novel form of huntingtin in medium spiny striatal neurons in Hdh^{Q92} and Hdh^{Q111} knock-in mice. *Hum. Mol. Genet.*, **9**, 503–513.
29. Wheeler, V.C., Gutekunst, C.A., Vrbanac, V., Lebel, L.A., Schilling, G., Hersch, S., Friedlander, R.M., Gusella, J.F., Vonsattel, J.P., Borchelt, D.R. *et al.* (2002) Early phenotypes that presage late-onset neurodegenerative disease allow testing of modifiers in *Hdh* CAG knock-in mice. *Hum. Mol. Genet.*, **11**, 633–640.
30. Gesquiere, L., Loreau, N. and Blache, D. (2000) Role of the cyclic AMP-dependent pathway in free radical-induced cholesterol accumulation in vascular smooth muscle cells. *Free Radic. Biol. Med.*, **29**, 181–190.
31. Levine, M.S., Klapstein, G.J., Koppel, A., Gruen, E., Cepeda, C., Vargas, M.E., Jokel, E.S., Carpenter, E.M., Zanjani, H., Hurst, R.S. *et al.* (1999) Enhanced sensitivity to *N*-methyl-D-aspartate receptor activation in transgenic and knockin mouse models of Huntington's disease. *J. Neurosci. Res.*, **58**, 515–532.
32. Tabrizi, S.J., Workman, J., Hart, P.E., Mangiarini, L., Mahal, A., Bates, G., Cooper, J.M. and Shapira, A.H.V. (2000) Mitochondrial dysfunction and free radical damage in the Huntington R6/2 transgenic mouse. *Ann. Neurol.*, **47**, 80–86.
33. Mantamadiotis, T., Lemberger, T., Bleckmann, S.C., Kern, H., Kretz, O., Martin Villalba, A., Tronche, F., Kellendonk, C., Gau, D., Kapfhammer, J. *et al.* (2002) Disruption of CREB function in brain leads to neurodegeneration. *Nat. Genet.*, **31**, 47–54.
34. Hardingham, G.E., Cruzalegui, F.H., Chawla, S. and Bading, H. (1998) Mechanisms controlling gene expression by nuclear calcium signals. *Cell Calcium*, **23**, 131–134.
35. Herzig, R.P., Scacco, S. and Scarpulla, R.C. (2000) Sequential serum-dependent activation of CREB and NRF-1 leads to enhanced mitochondrial respiration through the induction of cytochrome c. *J. Biol. Chem.*, **275**, 13134–13141.
36. Kadenbach, B., Huttemann, M., Arnold, S., Lee, I. and Bender, E. (2000) Mitochondrial energy metabolism is regulated via nuclear-coded subunits of cytochrome c oxidase. *Free Radic. Biol. Med.*, **29**, 211–221.
37. Wheeler, V.C., Auerbach, W., White, J.K., Srinidhi, J., Auerbach, A., Ryan, A., Duyao, M.P., Vrbanac, V., Weaver, M., Gusella, J.F. *et al.* (1999) Length-dependent gametic CAG repeat instability in the Huntington's disease knock-in mouse. *Hum. Mol. Genet.*, **8**, 115–122.
38. Persichetti, F., Carlee, L., Faber, P.W., McNeil, S.M., Ambrose, C.M., Srinidhi, J., Anderson, M., Barnes, G.T., Gusella, J.F. and MacDonald, M.E. (1996) Differential expression of normal and mutant Huntington's disease gene alleles. *Neurobiol. Dis.*, **3**, 183–190.
39. Au, J.L., Su, M.H. and Wientjes, M.G. (1989) Extraction of intracellular nucleosides and nucleotides with acetonitrile. *Clin. Chem.*, **35**, 48–51.
40. Grune, T., Siems, W., Gerber, G., Tikhonov, Y.V., Pimenov, A.M. and Toguzov, R.T. (1991) Changes of nucleotide patterns in liver, muscle and blood during the growth of Ehrlich ascites cells: application of the reversed-phase and ion-pair reversed-phase high-performance liquid chromatography with radial compression column. *J. Chromatogr.*, **563**, 53–61.